Europe PMC Funders Group
Author Manuscript
Sci Signal. Author manuscript; available in PMC 2018 March 05.

Published in final edited form as:
Sci Signal. ; 5(252): ra87. doi:10.1126/scisignal.2003365.

Lack of PTPN22 increases LFA-1-dependent adhesion of Murine Regulatory T Cells improving their regulatory Function

Rebecca J Brownlie[1], **Lisa A Miosge**[2,*], **Demetrios Vassilakos**[2,†], **Lena M Svensson**[3,4], **Andrew Cope**[3], and **Rose Zamoyska**[1,‡]

[1]Institute for Immunology and Infection Research, The University of Edinburgh, West Mains Rd, Edinburgh EH9 3JT UK

[2]Molecular Immunology, National Institute for Medical Research, Mill Hill, London NW7 1AA UK

[3]Academic Department of Rheumatology, Division of Immunology, Infection and Inflammatory Diseases, King's College School of Medicine, Guy's Campus, King's College London, London SE1 1UL, UK

[4]Department of Experimental Medical Sciences, Immunology Section, Lund University, Lund, Sweden

Abstract

The cytoplasmic phosphatase PTPN22 (protein tyrosine phosphatase non-receptor type 22) plays a key role in regulating lymphocyte homeostasis, which ensures that the total number of lymphocytes in the periphery is kept more or less constant. Mutations in *PTPN22* confer an increased risk of developing autoimmune diseases. The precise function of PTPN22 and how mutations contribute to autoimmunity is controversial. Loss of function mutations in *PTPN22* are associated with increased numbers of effector T cells and autoreactive B cells in humans and mice; however, the complete absence of *PTPN22* in mice does not result in spontaneous autoimmunity. We found that PTPN22 was a key regulator of regulatory T cell (Treg) function by fine-tuning the functions of the T cell receptor (TCR) and integrins. *PTPN22*$^{-/-}$ Tregs were more potent suppressors than were wild-type Tregs, and they suppressed the activity of *PTPN22*$^{-/-}$ effector T cells and maintained tolerance. Mechanistically, *PTPN22*$^{-/-}$ Tregs showed increased IL-10 production and elevated LFA-1 mediated adhesion, processes critical for Treg function. This previously undiscovered role of *PTPN22* in regulating integrin signaling and Treg function could prove to be a useful therapeutic target for manipulating Treg function in human disease.

‡To whom correspondence should be addressed. rose.zamoyska@ed.ac.uk.
*Current address: Department of Immunology, The John Curtin School of Medical Research, Australian National University, Canberra, Australia.
†Current address: Immunology Department, Epsom and St Helier University Hospitals NHS Trust, Surrey, SM5 1AA UK.

Author contributions: R.B. performed most of the experiments and analyzed data; L.M. designed and executed the knockout mouse strategy; D.V. helped with knockout mouse generation; L.S. performed experiments; A.C. and R.Z. designed experiments and analyzed data; and R.B. and R.Z. wrote the manuscript.

Competing interests: The authors declare no competing financial interests.

Europe PMC Funders Author Manuscripts
Europe PMC Funders Author Manuscripts

Europe PMC Funders Author Manuscripts

Europe PMC Funders Author Manuscripts

Introduction

Regulation of effector T cell responses is essential for maintaining immune homeostasis and tolerance. Failure to inhibit immune responses increases the risk of the development of autoimmunity and tumors. Phosphatases are key molecules that curtail T cell receptor (TCR) signaling, and one hematopoietic phosphatase, protein tyrosine phosphatase non-receptor type 22 (PTPN22, also known as Lyp in humans and PEP in mice) has a prominent role in inhibiting the activity of proximal tyrosine kinases that are activated by TCR engagement (1). The primary substrates of PTPN22 are the activating tyrosine residues on the Src family kinases (SFKs) Lck and Fyn, and their immediate target, ζ chain–associated protein kinase of 70kD (Zap70) (2, 3).

The importance of PTPN22 in regulating immune cell function is apparent from the numerous studies that confirm a strong link between a variant of PTPN22, R620W, and the development of autoimmune diseases (4–6). Controversy has surrounded the effect of this single nucleotide polymorphism on PTPN22 function, with some studies suggesting that PTPN22-R620W is a loss-of-function variant associated with increased T cell signaling (7, 8), whereas others suggest the opposite, namely that the PTPN22-R620W allelic variant is a hypermorph that results in decreased TCR signaling (9–11). A study of knock-in mice expressing the PTPN22 variant homolog (R619W) suggested that this mutation represents a loss of PTPN22 function because of the increased instability of the protein due to accelerated protease and proteosomal degradation (7). The abundance of PTPN22 seems to be critical to the cell, because an increase in the amount of PTPN22 is linked to the increased survival of B cells in chronic lymphocytic leukemia (12).

To understand how PTPN22 functions as a general autoimmune susceptibility locus, it is fundamental to gain a deeper understanding of the role of this protein in regulating immune cell responses. Healthy and autoimmune individuals with the major *PTPN22*^{C1858T} variant allele show increased numbers of effector and memory T cells (10) and autoreactive B cells (13). An increase in the number of cells in the effector and memory pool is associated with a predisposition to autoimmunity; however, tolerance is maintained in many *PTPN22*^{C1858T} carriers, indicating a more complex role for PTPN22.

Previously, a *Ptpn22* knockout mouse was reported (14), and despite the observation that these mice had increased numbers of effector and memory T cells and B cells compared to those of wild-type mice, together with more germinal centers and increased serum immunoglobulin concentrations, surprisingly, there were no signs of spontaneous autoimmunity. However, loss of PTPN22 cooperates with a mutant CD45 E613R protein (a phosphatase that modulates SFK activity), resulting in autoimmune disease in double mutant mice (8), which suggests that compound mutations might contribute to the autoimmune phenotypes associated with mutant *PTPN22* alleles. Here, we generated a *Ptpn22* knockout mouse (*Ptpn22*$^{-/-}$) strain, and found that loss of PTPN22 resulted in a substantial increase in the number of peripheral Tregs. In co-transfer experiments, we showed that *Ptpn22*$^{-/-}$ Tregs were more suppressive than their wild-type counterparts in vivo. Autoimmune colitis induced by *Ptpn22*$^{-/-}$ effector T cells, which were more pathogenic than wild-type effector T cells, was controlled by *Ptpn22*$^{-/-}$, but not wild-type, Tregs. *Ptpn22*$^{-/-}$ Tregs had an increased

Europe PMC Funders Author Manuscripts

Europe PMC Funders Author Manuscripts

propensity to secrete immunosuppressive cytokines compared to wild-type Tregs, and they showed enhanced activation of the integrin lymphocyte function-associated antigen-1 (LFA-1). The TCR-dependent increase in the extent of integrin-mediated adhesion through the activation of the guanosine triphosphatase (GTPase) Rap1 is critical for Treg function, whereas canonical TCR signals, such as activation of extracellular signal–regulated kinase (ERK) and Ca^{2+} flux, are entirely dispensable (15). We found that Rap1 phosphorylation was increased in the absence of PTPN22, pointing to a previously uncharacterized role for PTPN22 in modulating a pathway that links TCR signaling to inside-out integrin activation. Overall, we showed that PTPN22 activity is critical for the maintenance of immune homeostasis by regulating both effector and regulatory T cell function in vivo.

Results

Loss of PTPN22 leads to disruption of T cell homeostasis

First, we generated a *Ptpn22*$^{-/-}$ mouse strain (fig. S1, A to C). PTPN22 protein was ablated in homozygous *Ptpn22*$^{-/-}$ mice, as determined by Western blotting analysis (fig. S1D) and confirmed by the inability of two different anti-PEP (PTPN22) polyclonal antisera to immunoprecipitate PTPN22 protein from *Ptpn22*$^{-/-}$ splenocytes (fig. S1E). PTPN22 physically interacts with the kinase Csk (2). Immunoprecipitation of PTPN22 coimmunoprecipitated Csk from wild-type splenocytes, but not from *Ptpn22*$^{-/-}$ splenocytes (fig. S1F).

Overall, the phenotype of our *Ptpn22*$^{-/-}$ mice was similar to that of the strain reported previously (14). On a C57Bl/6 background, we saw no changes in thymocyte selection as a result of *Ptpn22* loss, unlike the slight increase in the selection of mature thymocytes noted in TCR transgenic strains (14). Wild-type and *Ptpn22*$^{-/-}$ mice had similar proportions and absolute numbers of $CD4^{-}CD8^{-}$ double negative (DN), $CD4^{+}CD8^{+}$ double positive (DP), and CD4 and CD8 single positive (SP) thymocytes (fig. S2A). In addition, the proportions and numbers of cells identified as undergoing positive selection by detection of the increased cell-surface abundance of CD69, CD5, and the TCR were unchanged in either strain (fig. S2, B and C). As described previously (8), CD5 abundance was slightly increased on pre-selection DP thymocytes from *Ptpn22*$^{-/-}$ mice; however, this distinction was not maintained on the positively selecting subset. Differences in the numbers of peripheral T cells and their cell-surface phenotypes were apparent when *Ptpn22*$^{-/-}$ and wild-type mice were compared (14). The numbers of both CD4+ and CD8+ effector memory and effector cells were four-fold greater in the lymph nodes of *Ptpn22*$^{-/-}$ mice compared to those of wild-type mice (fig. S3A and B), and more *Ptpn22*$^{-/-}$ T cells than wild-type T cells were characterized as $CD44^{hi}$ $CD62L^{lo}$, consistent with an effector or memory phenotype, which became more apparent with age.

The ratio of naive to memory T cells is normally maintained under tight homeostatic control in the periphery (16). To assess whether the increased representation of effector and memory T cells in *Ptpn22*$^{-/-}$ mice resulted from a cell-intrinsic failure of *Ptpn22*$^{-/-}$ T cells to obey homeostatic cues, we compared the ability of wild-type and *Ptpn22*$^{-/-}$ T cells to increase in number in vivo with a model of lymphopenia-induced proliferation. Naïve T cells from young wild-type ($CD45.1^{+}$) and *Ptpn22*$^{-/-}$ ($CD45.2^{+}$) mice, which had similar amounts of

Europe PMC Funders Author Manuscripts

Europe PMC Funders Author Manuscripts

CD44 and CD25, were labeled with carboxyfluorescein succinimidyl ester (CFSE) and injected intravenously (i.v.) into *Rag1*$^{-/-}$ recipient mice at a 1:1 ratio (Fig. 1A). After 14 days, we retrieved the lymph nodes and quantified the proportions of wild-type and *Ptpn22*$^{-/-}$ T cells. We found that there was a statistically significant increase in the ratio of CD45.2:CD45.1 CD4^{+} and CD8^{+} T cells, which indicated increased proliferation, survival, or both of *Ptpn22*$^{-/-}$ T cells compared to wild-type T cells in vivo (Fig. 1A). Because lymphopenia-induced proliferation is driven by a combination of signals from the TCR and cytokines (16), these data indicate that PTPN22 modulated these signals to maintain homeostatic balance between the naïve cell pool and the effector and memory cell pool. Quantitative reverse transcription polymerase chain reaction (RT-PCR) analysis showed that *Ptpn22* mRNA abundance was substantially increased in CD44^{hi} cells compared to that in thymocytes or naive CD44^{lo} cells (Fig. 1B). The increase in PTPN22 abundance in wild-type CD44^{hi} T cells and the preferential increase in the number of of *Ptpn22*$^{-/-}$ T cells support a key role for this phosphatase in regulating homeostasis of the pool of effector and memory T cells.

Ptpn22$^{-/-}$ mice had increased numbers of germinal centers compared to those of wild-type mice, and had an accumulation of T helper 2 (T_H2)-associated immunoglobulin (Ig) isotypes, but did not develop autoimmunity (14). We asked whether immunization with a strong T_H2-inducing antigen, *Schistosoma mansoni* egg antigen (SEA), could break tolerance in *Ptpn22*$^{-/-}$ mice. We chose a T_H2-inducing antigen because defects in linker of activated T cells (LAT) (17) and nuclear factor of activated T cells (NFAT) (18) result in T_H2 lymphoproliferative disorders, which suggests that altered TCR signaling predisposes to defects in the T_H2 arm of the immune response. SEA-specific Ig amounts were comparable between wild-type and *Ptpn22*$^{-/-}$ mice up to 2 months after immunization (Fig. 1C). Furthermore, whereas the total amount of serum Ig in *Ptpn22*$^{-/-}$ mice was increased compared to that in wild-type mice (fig. S4), as described previously (14), we found no evidence of autoimmunity in the immunized mice or cohorts of aged (> 6 month old) *Ptpn22*$^{-/-}$ mice.

PTPN22 abundance determines Treg numbers and function

We reasoned that regulatory processes might restrain the enhanced responsiveness in *Ptpn22*$^{-/-}$ mice (19). Proportions of CD25^{+}FoxP3^{+} Tregs in young (~6-week) *Ptpn22*$^{-/-}$ mice and both the proportions and absolute numbers of Tregs in the lymph node and spleen were substantially increased in aged (> 6 month old) *Ptpn22*$^{-/-}$ mice as compared to wild-type mice (Fig. 2A). Increased numbers of Tregs could be explained by the increased selection of “natural” thymic Tregs (nTregs), increased induction of inducible Tregs (iTregs) in the periphery, or increased expansion in number and survival of either or both of these populations. We found that numbers of FoxP3^{+} cells were not increased in the thymi of young or old *Ptpn22*$^{-/-}$ mice compared to those in wild-type mice, suggesting comparable selection of nTregs in both strains (Fig. 2B). iTregs can be induced in vitro through stimulation of of naïve FoxP3^{-} CD4+ T cells through the TCR (with antibody against CD3) and the coreceptor CD28 in the presence of TGF-β and interleukin-2 (IL-2) (20). iTreg differentiation conditions with low concentrations of anti-CD3 antibody generated more FoxP3^{+} cells from *Ptpn22*$^{-/-}$ precursors than were derived from wild-type cells (Fig. 2C).

Europe PMC Funders Author Manuscripts

Europe PMC Funders Author Manuscripts

Therefore, increased numbers of Tregs in *Ptpn22*$^{-/-}$ mice may, in part, result from an increased propensity of naïve T cells to differentiate to this lineage, although in *Ptpn22*$^{-/-}$ mice we did not observe a disproportionate accumulation of Tregs in mesenteric lymph nodes, a key site of iTreg induction (21).

PTPN22 was recently identified as a target gene whose expression is inhibited by FoxP3 (22). Indeed, wild-type CD44^{int}CD25^{+}CD4^{+} cells taken directly ex vivo (~90% FoxP3^{+}) had a substantially decreased amount of *PTPN22* mRNA compared to that of CD44^{hi}CD25^{-} T cells (Fig. 1B). We asked whether PTPN22 also regulated the suppressive capacity of Tregs by comparing the potency of wild-type and *Ptpn22*$^{-/-}$ Tregs in an in vivo T cell suppression assay. Naive wild-type CD4^{+} T cells (CD45.1^{+}) were mixed in a 2:1 ratio with either wild-type or *Ptpn22*$^{-/-}$ lymph node–derived Tregs (CD45.2^{+}) and injected i.v. into *Rag1*$^{-/-}$ recipient mice (Fig. 3A). After 14 days, we analyzed lymph nodes for the presence of both CD45.1^{+}FoxP3^{+} and CD45.2^{+}FoxP3^{+} donor cells. Co-transfer of either wild-type or *Ptpn22*$^{-/-}$ Tregs suppressed the expansion in number of naive CD45.1^{+} T cells, because we recovered fewer cells from these recipients, and there was a statistically significant reduction in naive CD45.1^{+} T cells between mice that had received *Ptpn22*$^{-/-}$ Tregs compared to those that received wild-type Tregs (Fig. 3B and C). These data demonstrate that *Ptpn22*$^{-/-}$ Tregs are more suppressive than wild-type Tregs in vivo. The enhanced suppressive capacity of *Ptpn22*$^{-/-}$ Tregs compared to that of wild-type Tregs was on a cell per cell comparison, because the numbers of recovered Tregs were similar between the two groups (Fig. 3C), indicating that the suppressive effect was a cell-intrinsic property conferred by the lack of PTPN22.

It was possible that the enhanced suppressive capability of *Ptpn22*$^{-/-}$ Tregs was simply an indirect consequence of *Ptpn22*$^{-/-}$ Tregs residing in a more inflammatory environment generated by the expanded pool of *Ptpn22*$^{-/-}$ effector T cells. Alternatively, loss of PTPN22 could intrinsically benefit Tregs, enabling them to outperform their wild-type counterparts. Indeed the demonstration that FoxP3 targets *PTPN22* expression suggests that inhibition of *PTPN22* expression might be required for optimal Treg function. To address this question, we repeated the in vivo T cell suppression assay with young thymic nTregs, which had not been exposed to the expanded peripheral effector T cell pool. Additionally, we assessed the suppression of *Ptpn22*$^{-/-}$ CD4^{+} T cells, reasoning that if the increased efficacy of *Ptpn22*$^{-/-}$ Tregs was a result of their environment, then wild-type Tregs should be equally efficient in the same environment. We mixed naïve *Ptpn22*$^{-/-}$ CD4^{+} T cells in a 4:1 ratio with either wild-type or *Ptpn22*$^{-/-}$ thymic Tregs, injected them i.v. into *Rag1*$^{-/-}$ recipient mice, and analyzed them 19 days later (Fig. 3D-E). We found that wild-type and *Ptpn22*$^{-/-}$ nTregs suppressed the expansion of *Ptpn22*$^{-/-}$ naïve T cells. *Ptpn22*$^{-/-}$ nTregs were substantially more suppressive than wild-type nTregs (Fig. 3D), and Treg recovery was comparable regardless of genotype (Fig. 3E). These experiments confirmed that *Ptpn22*$^{-/-}$ Tregs were intrinsically more suppressive than wild-type Tregs and that this was not simply a response to the hyper-responsive immune environment created by the absence of PTPN22.

Given that wild-type Tregs have already reduced *PTPN22* expression compared to that of T effector cells, we asked whether Treg function could be modulated by changes in the expression of PTPN22. To this end we measured the suppressive activity of Tregs from

Europe PMC Funders Author Manuscripts

Europe PMC Funders Author Manuscripts

Ptpn22$^{+/-}$ heterozygous mice, which have a reduced amount of PTPN22 protein compared to that of wild-type mice (fig. S5A). Indeed, *Ptpn22*$^{+/-}$ mice showed an expansion in Treg number that was intermediate between that of wild-type mice and *Ptpn22*$^{-/-}$ mice (fig. S5B), and their potency in suppressing T cell responses in vitro was also intermediate between those of wild-type and *Ptpn22*$^{-/-}$ Tregs (fig. S5C). These data showed that even two-fold changes in PTPN22 abundance influenced both Treg production and function.

Ptpn22$^{-/-}$ mice do not develop spontaneous autoimmunity, which could be because of their more efficient Tregs. Although the major autoimmune-associated PTPN22 variant does not confer an increased risk of inflammatory bowel disease in man (23, 24), the well-characterized model of colitis in mice (25) provides an efficient indication of Treg function in vivo. It is one of the few models that enable assessment of the pathogenicity of effector T cells independently from Treg function, so we used the colitis model to investigate whether *Ptpn22*$^{-/-}$ T cells were inherently more pathogenic than wild-type T cells and whether this activity was regulated by *Ptpn22*$^{-/-}$ Tregs. In this model, the transfer of naive $CD4^{+}CD45RB^{hi}$ T cells alone into immunodeficient mice results in inflammation of the colon and weight loss that can be completely prevented by the co-administration of $FoxP3^{+}$ Tregs. We injected naïve wild-type or *Ptpn22*$^{-/-}$ $CD4^{+}$ T cells either alone or in combination with wild-type or *Ptpn22*$^{-/-}$ Tregs (in an 8:1 ratio) obtained from either the periphery or the thymus i.v. into *Rag1*$^{-/-}$ recipient hosts and then assessed weight loss for up to 76 days post-injection. When transferred alone, *Ptpn22*$^{-/-}$ T cells induced more severe colitis, with more rapid weight loss and greater mortality. than was induced when wild-type T cells alone were transferred (Fig. 4A and B). This was entirely consistent with a greater increase in the number of *Ptpn22*$^{-/-}$ T cells compared to that of wild-type cells under similar lymphopenic conditions in vivo that was seen in short-term assays (Fig. 1A). Pathological assessment confirmed that the type of pathology induced by wild-type and *Ptpn22*$^{-/-}$ CD4 T cells was similar (Fig. 4C). Wild-type Tregs were unable to protect mice from colitis induced by *Ptpn22*$^{-/-}$ T cells, despite being able to prevent disease induced by wild-type T cells. In contrast, *Ptpn22*$^{-/-}$ Tregs prevented colitis induced by *Ptpn22*$^{-/-}$ T cells, consistent with their enhanced suppressive activity, which was seen in short-term in vivo suppression assays (Fig. 3B-E). Both peripheral (Fig. 4A) and thymic (Fig. 4B) *Ptpn22*$^{-/-}$ Tregs effectively suppressed colitis induced by *Ptpn22*$^{-/-}$ $CD4^{+}CD45RB^{+}$ T cells, whereas equivalent wild-type populations could suppress only wild-type $CD4^{+}CD45RB^{+}$ T cells, suggesting that tolerance is maintained in *Ptpn22*$^{-/-}$ mice because their Tregs are intrinsically more effective than those of wild-type mice.

Ptpn22$^{-/-}$ Tregs display an activated phenotype and secrete increased amounts of IL-10

Tregs exert their suppressive functions through various effector mechanisms, such as consumption of IL-2, production of IL-10, and increasing the abundance of immunomodulatory molecules, such as cytotoxic T-lymphocyte antigen 4 (CTLA-4) (26). Phenotypic analysis showed that wild-type and *Ptpn22*$^{-/-}$ Tregs had similar amounts of surface CD25 and intracellular CTLA-4 and glucocorticoid-induced tumor necrosis factor receptor (GITR) (Fig. 5A). In contrast, *Ptpn22*$^{-/-}$ Tregs from lymph nodes and spleen had increased amounts of surface CD103 and CD73 and decreased amounts of CD62L compared to those of wild-type Tregs (Fig. 5A), consistent with an effector phenotype (27, 28). This

Europe PMC Funders Author Manuscripts

Europe PMC Funders Author Manuscripts

phenotype was also influenced by the abundance of PTPN22, because *PTPN22*$^{+/-}$ mice showed intermediate amounts of these molecules (fig. S5D).

Given the critical role of IL-2 in maintaining the homeostasis of Tregs (29), we compared the responses of wild-type and *Ptpn22*$^{-/-}$ Tregs to IL-2. Intracellular staining showed that the extent of IL-2–induced phosphorylation of signal transducer and activator of transcription 5A (STAT5) in wild-type and *Ptpn22*$^{-/-}$ Tregs was comparable (Fig. 5B). These results indicated that PTPN22 does not regulate IL-2–induced JAK-STAT signaling in Tregs. By contrast, a greater proportion of *Ptpn22*$^{-/-}$ Tregs than wild-type Tregs secreted IL-10, an important immunosuppressive cytokine (30), upon stimulation with phorbol ester and ionomycin (Fig. 5C). Together, these data showed that the increased suppressive capability of *Ptpn22*$^{-/-}$ Tregs as compared to that of wild-type Tregs was associated with an activated cell-surface phenotype and a greater capacity for the production of immunosuppressive IL-10.

Lack of PTPN22 increases LFA-1-dependent adhesion but not proximal TCR signaling in Tregs

Tregs have a decreased responsiveness to stimulation through the TCR and adopt an “anergic” state in vitro (31, 32). However, in comparison to how much is known about conventional T cells, relatively little is known about the signaling events that control Treg function, and specifically how PTPN22 might influence Treg signaling. We compared the amounts of specific phosphorylated proteins in wild-type and *Ptpn22*$^{-/-}$ T cells after they underwent antibody-mediated cross-linking of CD3 and CD4. *Ptpn22*$^{-/-}$ effector T cells (fig. S6) had increased amounts of Zap70 phosphorylated at residues Tyr^{319} and Tyr^{493}, Shc phosphorylated at Tyr^{239} and Tyr^{240}, and ERK phosphorylated at Thr^{202} and Tyr^{204}, indicating the increased responsiveness of these cells to TCR stimulation compared with that of wild-type effector cells, as was described previously (14). In contrast, phosphorylation of these same tyrosine residues in Zap70, Shc, and ERK in Tregs was unaffected by the absence of PTPN22 (Fig. 6A). Consistent with these data, crosslinking of CD3 and CD4 induced comparable Ca^{2+} flux in wild-type and *Ptpn22*$^{-/-}$ Tregs (Fig. 6B). Together, these data indicate that, although proximal TCR signaling is increased in *Ptpn22*$^{-/-}$ $CD4^+$ effector T cells compared to their wild-type counterparts, lack of PTPN22 does not substantially alter proximal TCR signaling in Tregs.

A report (15) demonstrated that the kinase function of Zap70 and many subsequent downstream signaling pathways were dispensable for Treg-mediated suppression. Instead, Zap70 acted as a scaffold for the propagation of a signaling cascade involving the small guanosine triphosphatase (GTPase) Rap1. This Zap70 kinase-independent pathway ultimately resulted in enhanced LFA1-mediated adhesion of Tregs to intracellular adhesion molecule 1 (ICAM1) and was sufficient for the suppressive activity of Tregs (15). We hypothesized that PTPN22 played a role in regulating this Zap70 scaffold-mediated, LFA-1–dependent pathway that is critical for Treg function. Flow cytometric analysis showed that LFA-1 abundance was greater in resting *Ptpn22*$^{-/-}$ $FoxP3^+$ Tregs than in wild-type Tregs, which was maintained upon cross-linking of CD3 and CD4 (Fig. 7A and B). Because of difficulties in obtaining sufficient numbers of Tregs for biochemical analysis, we

Europe PMC Funders Author Manuscripts

Europe PMC Funders Author Manuscripts

demonstrated the direct involvement of PTPN22 with this pathway in experiments with effector T cells in which *Ptpn22*$^{-/-}$ effector T cells showed increased active Rap1 compared to that of wild-type cells upon cross-linking of CD3 and CD4 (Fig. 7C and D). To assess the functional effect of increased LFA-1 abundance, we sorted wild-type and *Ptpn22*$^{-/-}$ Tregs from lymph nodes and activated them with the chemokine stromal cell–derived factor 1 (SDF-1, also known as CXCL12), to induce an inside-out conformational change in LFA-1, before seeding the cells on ICAM1-coated plates. Adherent cells were visualized by interference reflection microscopy (IRM). It was apparent that *Ptpn22*$^{-/-}$ Tregs made larger areas of contact on ICAM-coated surfaces than did wild-type Tregs, confirming a functional effect of the increased LFA-1 abundance on *Ptpn22*$^{-/-}$ Tregs (Fig. 7E and F).

Discussion

The failure of *Ptpn22*$^{-/-}$ mice to develop autoimmune syndromes was puzzling given the expansion in these mice in the number of effector and memory T cells, indicating their lack of constraint by normal homeostatic cues. We showed that a possible explanation for the maintenance of tolerance in these mice was that dysregulation of the effector T cell pool was matched by a concomitant increase in Treg efficacy. *Ptpn22*$^{-/-}$ Tregs exhibited enhanced LFA-1–mediated adhesion and increased IL-10 production, processes that are critical for Treg function (30, 33, 34). We provide evidence that PTPN22 regulates LFA-1 activation through a pathway involving TCR-dependent Rap1 activation. Together, these data show that PTPN22 is important for the maintenance of immune homeostasis by regulating both effector and regulatory T cell function in vivo.

Ptpn22 is a major target of FoxP3 (22). *Ptpn22* expression in stimulated Tregs is considerably lower than in activated T cells, which is consistent with FoxP3-mediated suppression of its target genes (22), and suggests that PTPN22 protein might impede Treg function. We found that *PTPN22* mRNA was substantially decreased in CD25^{+}CD44^{hi} T cells ex vivo compared with that in CD25^{-}CD44^{hi} T cells. Nonetheless, in comparison to naïve T cells, *PTPN22* mRNA was increased in CD25^{+} cells, although we cannot exclude the possibility of contamination by the small percentage (~10%) of cells within the CD25^{+} gate that are activated T cells. However, the intermediate phenotypes that we observed with heterozygous mice indicated that the abundance of PTPN22 was critical to balance Treg and effector T cell signaling and function. These data are consistent with a less stable form of the protein, as found with the disease associated variant (7), having an effect on susceptibility to autoimmunity even in heterozygous individuals. Furthermore, it has been reported that PTPN22 is increased in abundance in certain malignant B cells, conferring them with resistance to apoptosis (12) and highlighting the critical importance of PTPN22 abundance within the cell.

The signals that regulate Treg function are poorly understood. Activated Tregs can be non-antigen-specific and have suppressor function, while bypassing conventional TCR signal transduction pathways (15). However, activation of Src family kinases is critical for Treg function, because Lck phosphorylates tyrosine residues in the linker region of Zap70 that serve an adaptor function for the recruitment of CrkII-C3G (CrkII, v-crk sarcoma virus CT10 oncogene homolog; C3G, Rap1 guanine nucleotide exchange factor 1, also known as

Europe PMC Funders Author Manuscripts

Europe PMC Funders Author Manuscripts

RAPGEF1) and the activation of Rap1(15), which is important for generating “inside-out” signals that increase adhesion between LFA-1 and ICAM1 adhesion. In addition, Src kinase–associated protein of 55 kD homolog (SKAP-HOM), an adaptor protein that is involved in integrin activation, is a substrate for Ptpn22 (35). Our data showed that PTPN22 regulated Rap1 activity in T cells, and that *Ptpn22*$^{-/-}$ Treg cells had an increased abundance of LFA-1 and made more extensive contacts with ICAM1-coated surfaces than did wild-type Tregs, suggesting a mechanism by which these cells were more suppressive.

Tregs suppress target cells by various mechanisms: those that depend on cell-cell contact; the killing of antigen-presenting cells (APCs) or responder T cells; mechanisms mediated by soluble factors, such as IL-10, transforming growth factor–β (TGF-β), IL-35, and galectin-1; and by the deprivation of cytokines, including IL-2 (26). It is likely that several mechanisms act synergistically to confer Tregs with suppressive function; however, a general property for harnessing suppressor activity is the ability of Tregs to migrate to sites of inflammation, as well as their capacity to form close contacts with target cells. We found that *Ptpn22*$^{-/-}$ Tregs had an effector phenotype characterized by reduced CD62L abundance and increased integrin CD103 (αEβ7) abundance, and that they made substantially larger areas of contact with surface-bound ICAM1 than did wild-type Tregs, confirming a functional consequence of increased LFA-1 abundance, and suggesting that *Ptpn22*$^{-/-}$ Tregs may be able to traffic more efficiently to sites of inflammation and form closer or more stable contacts with their target cells. Combined with an increased propensity to secrete the immunosuppressive cytokine IL-10, these data give a potential mechanistic basis for the increased functionality of *Ptpn22*$^{-/-}$ Tregs.

Susceptibility to autoimmune disease has been linked with changes in the T cell repertoire that is selected in the thymus. It is unclear whether loss of *Ptpn22* has a substantial efffect on this process, because PTPN22 abundance is lower in the thymus than in the periphery. *Ptpn22*$^{-/-}$ DP thymocytes have marginally enhanced signaling, positively selecting slightly more TCR transgenic cells than occurs in the wild-type thymus (14), and they have more CD5, which is associated with enhanced responsiveness. We found that the abundance of CD5 was increased on pre-selection DP cells, but was normalized in the post-selection SP cells. Numbers of nTregs were not increased in the *Ptpn22*$^{-/-}$ thymus compared to those in the wild-type thymus, suggesting that the larger numbers of Tregs in *Ptpn22*$^{-/-}$ mice were not a result of increased thymic selection. These data apparently contradict a report showing increased proportions of nTregs in *Ptpn22*$^{-/-}$ mice (36). We also observed similar increased proportions in some individuals; however, when we analyzed the data from >20 animals, we found these small fluctuations did not translate into a statistically significant difference in the absolute numbers of Tregs between wild-type and *Ptpn22*$^{-/-}$ mice. A report that suggested that activated CD4^{+} effector T cells in an autoimmune setting boost the expansion in number of Tregs through a mechanism dependent on tumor necrosis factor α (TNF-α) (37) is likely to be pertinent given the increase in numbers of both effector T cells and Tregs in *Ptpn22*$^{-/-}$ mice. However, in addition to regulating peripheral Treg numbers, PTPN22 has a more fundamental role in Treg function, because even thymic *Ptpn22*$^{-/-}$ Tregs were more suppressive than their wild-type counterparts, indicating that they were intrinsically more potent.

Europe PMC Funders Author Manuscripts

Europe PMC Funders Author Manuscripts

The most important physiological substrates of PTPN22 in both effector and regulatory T cells remain unclear. PTPN22 is thought to function by dephosphorylating the activating Tyr^{394} residue of Lck (14). This ability is shared with additional phosphatases, including CD45 (38), PTP-PEST (39) and SHP1 (40). PTPN22 appears to have a more prominent role in activated T cells than in naïve T cells, because *PTPN22* mRNA amounts were higher in effector T cells, whereas PTP-PEST and CD45 are more important in regulating Lck phosphorylation in naïve T cells (38, 41), which suggests that individual phosphatases have key roles at different stages of T cell differentiation. Increased PTPN22 abundance in effector T cells might be a feedback mechanism to limit the extent of their activation. Functional redundancy of these T cell–resident phosphatases was indicated from the observation that PTPN22 and CD45 doubly deficient mice develop an autoimmune lupus-like disease (8).

It remains contentious whether the autoimmune-associated R620W substitution increases or decreases PTPN22 activity. It was shown that this mutation destabilized PTPN22 protein, reducing its abundance (7). The observation that, as with *Ptpn22*$^{-/-}$ mice, effector T cell pools are increased in number in both mice and humans that express the PTPN22 R620W variant (7, 10) supports the notion that this variant is a hypomorph. Moreover, in addition to increased numbers of effector T cells, $PTPN22^{R619W}$ knockin mice have increased numbers of CD25+ CD44med T cells, indicative of increased Tregs (7).. However, it remains to be determined whether the $PTPN22^{R619W}$ variant results in Tregs that are as suppressive as *Ptpn22*$^{-/-}$ Tregs. If not, then $PTPN22^{R619W}$ Tregs may not be capable of maintaining tolerance as effectively.

In summary, our data show that PTPN22 plays an important role in Treg generation and function. Loss of PTPN22 increased the suppressive capacity of Tregs that, in turn, restrained the enhanced responsiveness of effector T cells in *Ptpn22*$^{-/-}$ mice. Overall, PTPN22 activity is critical for the maintenance of immune homeostasis by regulating both effector and regulatory T cell function in vivo. These findings indicate that monitoring the impact of autoimmune associated *PTPN22* mutations on Treg function in man could be an important predictor of autoimmune disease.

Materials and Methods

Mice

LoxP-flanked (floxed) *Ptpn22* alleles were generated as described in fig. S1. *Ptpn22* fl/+ mice were bred with PC3-Cre mice and backcrossed to C57BL/6 mice for four generations. Mice were bred and maintained at Edinburgh University facility under U.K. Home Office and local ethically approved guidelines. C57BL/6 (CD45.1hom and CD45.2hom), *Rag1*$^{-/-}$, OTI TCR transgenic and CD3ε$^{-/-}$ mice were bred and maintained at Edinburgh University facility under the U.K. Home Office and local guidelines.

Antibodies and flow cytometry

Specific antibodies, their conjugated fluorophores, and sources are as follows: CD3-bio, CD4-PerCP, CD4-bio, CD5-APC, CD8-PE, CD8-APC, CD25-PE, CD25-APC, CD62L-PE,

Europe PMC Funders Author Manuscripts

Europe PMC Funders Author Manuscripts

CD69-PE TCRbio, CD4-PerCP, CD4-bio, CD5-APC, CD8-PE, CD8-APC, CD25-PE, CD25-APC, CD62L-PE, CD69-PE were from BD Biosciences. I-Ab-bio, B220-bio, DX5-bio, Gr1-bio, CD11b-bio, CD11c-bio, CD44-FITC, CD44-APC, CD45.2-PE, CD103-bio, FoxP3-APC, and LFA-1-PE (clone M17/4) were from e-Bioscience. CD73-APC and CD39-PE were from Biolegend; CD4-AlexaFluor750 and CD8-PE-Texas Red were from Invitrogen; And CD45.1-FITC was from abcam. Antibodies against pSrc Y416, pLck Y505, pZap70 Y319, pZap70 Y493, and pERK T202/Y204 were from Cell Signaling Technology, and antibody against pShc Y239/240 was from Santa Cruz Biotechnology. FoxP3 staining was performed with the eBioscience FoxP3 staining kit. For intracellular staining of phosphorylated proteins, cells were fixed with BD Phosflow Lyse/Fix Buffer I and stained with phospho-specific antibodies in BD Phosflow Perm/Wash Buffer I (BD Biosciences). Non-conjugated antibodies were counterstained with Alexa Fluor 647–conjugated goat anti-rabbit antibodies (Molecular Probes). For staining of intracellular IL-10, mesenteric lymph node cells were labeled with PerCP-conjugated anti-CD4 and phycocrythrin (PE)-conjugated anti-CD25 antibodies before stimulation with phorbol 12, 13-dibutyrate (PDBU) (20 ng/ml) and ionomycin (0.5 μg/ml) with brefeldin A (1 μg/ml) for 4 hours. Cells were fixed with 2% paraformaldehyde (PFA), permeabilized with 0.5% saponin, and then stained for IL-10. Samples were acquired with an LSR II flow cytometer (BD Biosciences) and analyzed with FlowJo Software (Treestar).

T cell stimulation

Lymph node cells were stained with biotin-conjugated anti-CD3 (145-2C11) and biotin-conjugated anti-CD4 (RM4.5) antibodies for 20 min at 4°C, washed, and cross-linked with PerCP-conjugated streptavidin. To analyze Ca^{2+} flux, before stimulation, a 1:1 mix of WT (CD45.1) and *Ptpn22*$^{-/-}$ (CD45.2) $CD4^+$ cells were loaded with 2 μM indo-1-AM (Sigma-Aldrich) and then stained for surface markers. To monitor increases in LFA-1 abundance, T cells were stimulated for 2 hours at 37°C, stained with anti-LFA-1 antibody for 20 min, then fixed, and stained for FoxP3. Negative controls for staining for phosphorylated proteins were preincubated for 10 min with 1 μM PP2.

Analysis of pSTAT5

T cells were stimulated with IL-2 (1 ng/ml, R&D) for 15 min at 37°C and fixed with an equal volume of 4% PFA in phosphate-buffered saline (PBS) for 15 min at room temperature. Cells were washed twice in PBS, permeabilized with ice-cold 90% methanol overnight at -20°C and stained for pSTAT5 and surface antigens.

Purification of T cells

Lymph node T cells were purified by negative selection on a MACS column after labeling with biotinylated antibodies against I-A^b, B220, DX5, Gr1, CD11b, and CD11c and streptavidin-MACS beads (Miltenyl Biotech). Thymi were purified by complement lysis of $CD8^+$ thymocytes with antibody against CD8 (clone 3.168) and rabbit complement (Cedarlane). Pure populations of naïve T cells ($CD4^+CD25^-CD44^{lo}$ or $CD4^+CD25^-CD45RB^{hi}$) and Tregs ($CD4^+CD25^+$) were obtained by sorting.

Europe PMC Funders Author Manuscripts

Europe PMC Funders Author Manuscripts

Adoptive cell transfer

MACS-purified lymph node T cells labelled with 1 μM CFSE (Molecular Probes) for 10 min at room temperature were washed twice, and 4 x 10^6 cells were injected i.v. into *Rag1*$^{-/-}$ recipient mice. To analyze Treg function in vivo, sorted purified populations of naive CD45.1$^+$ (1 to 4 x 10^5 cells) together with CD45.2$^+$ Tregs (0.25 to 2 x 10^5 cells) were injected i.v. into *Rag1*$^{-/-}$ recipients and analyzed after 14 days. For colitis studies, mice were injected i.v. with 4 x 10^5 naïve CD4$^+$CD25$^-$CD45RB^{hi} T cells ± 5 x 10^4 Tregs and were monitored for signs of weight loss. Any mouse losing >20% of its initial starting weight or showing severe signs of disease was killed.

Immunization of mice with *Schistosoma mansoni* eggs

Groups of WT and *Ptpn22*$^{-/-}$ mice were immunized with 2000 *Schistosoma mansoni* eggs (kindly supplied by A MacDonald) i.p., and boosted with 1000 eggs 7 weeks later. Serum was collected weekly by tail bleeds and SEA-specific antibodies were assessed by ELISA.

Generation of Tregs

Highly pure (>98%) naïve CD4$^+$CD25$^-$ T cells were obtained by negative selection, as described earlier, after which they underwent positive selection with CD4$^+$ beads and MACS columns. Cells were cultured in 96-well plates in complete medium [IMDM (Invitrogen), 10% fetal calf serum (FCS), 100 U/ml penicillin, 100 U/ml streptomycin and 25 μM 2-mercaptoethanol (ME)] at 37°C. Cells were stimulated with anti-CD3 (0.01 to 0.1 μg/ml), anti-CD28, recombinant murine IL-2 (20 ng/ml), and recombinant human TGF-β1 (0.4 ng/ml, R&D Systems) for 3 days.

Quantitative RT-PCR analysis

Sorted (>98% pure) CD4$^+$CD25$^+$ Tregs, naïve CD4$^+$CD44^{lo}CD25$^-$ cells, and CD4$^+$CD44^{hi}CD25$^-$ effector T cells (2.5 x 10^5) were lysed for RNA extraction with Trizol (Invitrogen). Reverse transcription of RNA was performed with SuperScript III (Invitrogen). Quantitative PCR (qPCR) reactions were performed with TaqMan primers specific for mouse *Hprt* and *Ptpn22* (exon boundary 4 to 5; assay ID Mm00501231_g1, Applied Biosystems) and normalized to the abundance of *Hprt* mRNA.

LFA-1–mediated adhesion to surface-bound ICAM1 by IRM

CD4$^+$CD25^{hi} T cells were plated on μ-Slides VI (ibidi GmbH) coated with ICAM1 (R&D systems) at 37°C in Hanks' balanced salt solution/*N*-2-hydroxyethylpiperazine-*N*′-2-ethanesulfonic acid. Images of close substrate contact of the migrating cells were acquired from 10 to 30min with a LSM 510 Zeiss inverted confocal microscope with a 63× NA1.4 Plan-Apochromat oil immersion objective lens. For evaluation of adhesion status, the area of contact was measured with MetaMorph Offline 7.1 (Molecular Devices).

Rap1 assay

T cell effectors were generated in vitro (as described earlier) and stained with anti-CD3-biotin (145-2C11) and anti-CD4-biotin (RM4.5) antibodies (both at 10 μg/ml) for 20 min at 4°C, washed, and antibodies were cross-linked with avidin (0.5 μg/ml) for the indicated

Europe PMC Funders Author Manuscripts

Europe PMC Funders Author Manuscripts

times. 2 x 10^6 cells were used for each condition. Rap1-precipitation assays were performed according to the manufacturer's instructions (Thermo Scientific).

Generation of effector T cells in vitro

Splenocytes were stimulated in culture with Concanavalin A (ConA, 2.5 μg/ml, Sigma Aldrich) for 2 days, washed, and then cultured with IL-2 (2 ng/ml) for a further 4 days.

Southern blotting

DNA was extracted from embryonic stem (ES) cell clones by phenol extraction, and DNA (10 μg/ml) was digested with Bspq 1 at 50°C. Samples were resolved on a 0.7% agarose gel. The gel was then subjected to depurination (in 0.2 M HCl), denaturation (in 1.5 M NaCl, 0.5 M NaOH), and neutralization [in 1 M Tris (pH 7.4), 1.5 M NaCl] before Southern blotting with a TurboBlotter system (Whatman Schleicher & Schuell) onto a nylon membrane (Hybond-N; Amersham Biosciences). The transferred DNA was then fixed to the membrane by UV exposure before incubation with hybridization buffer (SSC; Invitrogen, 0.5% SDS, 0.2% Denharts, 1% denatured ssDNA; Sigma-Aldrich). Radiolabelled probes were added for 24 hours before washing and exposure to film for at least 24 hours before the film was developed with an X-ray processor.

Western blotting and immunoprecipitations

Cells were lysed in 1% Triton X-100, 0.5% *n*-dodecyl-*b*-D-maltoside, 50 mM Tris-HCl (pH 7.5), 150 mM NaCl, 20 mM EDTA, 1 mM NaF and 1 mM sodium orthovanadate containing protease inhibitors. Samples were separated by SDS-polyacrylamide gel electrophoresis. For immunoprecipitations, lysates were precleared with 20 μl protein A-sepharose (Sigma Aldrich) slurry before immunoprecipitation with anti-Ptpn22 rabbit serum (82.2, kindly supplied by A Veillette) and rabbit polyclonal anti-CSK (clone C-20; Santa Cruz Biotechnology) coupled to Sepharose beads. Immunoprecipitates were washed with lysis buffer, and proteins were transferred to polyvinylidene difluoride membranes (Millipore). Membranes were incubated in blocking reagent (LI-COR Biosciences) before Western blotting analysis with goat antibody against Lyp (AF3428; R&D Systems) or mouse anti-CSK antibody (clone 52; BD). Proteins were detected with secondary antibodies and visualized with an infrared imaging system (Odyssey; LI-COR Biosciences).

ELISA

Cytokines and serum antibodies were measured by ELISA with paired capture and detection antibodies [capture (RA6A2) and detection (XMG1.2)] anti-IFNγ antibody from BD and anti-Ig antibody from SouthernBiotech. Plates (NUNC Maxisorb) were washed with 0.05% Tween 20 in PBS and blocked with 1% BSA in PBS. For SEA ELISAs, plates (NUNC Maxisorp) were coated with 0.25 μg/well of SEA in 0.1 M sodium carbonate-bicarbonate buffer (pH 9.6), washed, and blocked with 1% BSA in PBS. Serum samples were analyzed by serial two-fold dilutions. Specific isotypes were detected with alkaline phosphatase–conjugated goat antibody against mouse Ig (SouthernBiotech). For all ELISAs, after the addition of 100 μl of TMB substrate solution (Sigma-Aldrich) and 100 μl of 0.1 M H_2SO_4, absorbance was read at 450 nm with a Laboratory Systems Multiskan Ascent plate reader.

Europe PMC Funders Author Manuscripts

Histological assessment of intestinal inflammation

Samples of lower intestine were fixed in 10% formalin solution. Paraffin-embedded sections were cut and stained with hematoxylin and eosin, and inflammation was scored in a blinded fashion.

In vitro suppression assay

Cultures of 5 x 10^4 OTI TCR-transgenic $CD8^+$ T cells, as responders, together with 2 x 10^5 peptide pulsed (with $OVA_{257-264}$ SIINFEKL peptide), irradiated $CD3\varepsilon^{-/-}$ spleen cells and titrated numbers of in vitro–generated Tregs from *Ptpn22*$^{+/+}$, *Ptpn22*$^{+/-}$, or *Ptpn22*$^{-/-}$ mice were set up in 96-well plates for 72 hours. IFN-γ was assessed by ELISA. Tregs were generated by culturing sorted $CD4^+CD25^+CD44^{lo}$ naïve T cells on plates coated with 0.5 μg/ml anti-CD3 and 5 μg/ml anti-CD28 antibodies in addition to 10 ng/ml TGFβ, 5 μg/ml anti-IL-4 antibody, and 10 μg/ml anti-IFN-γ antibody for 3 days, and then transferred to uncoated plates for a further 2 days before being used in suppression assays.

Statistical analysis

Statistical analysis was performed with Prism 5.0 (GraphPad Software). The non-parametric, two tailed, unpaired Student's *t* Test was used for all statistical comparisons, except for the survival curve analysis, for which a Log-rank (Mantel-Cox) test was used.

Supplementary Material

Refer to Web version on PubMed Central for supplementary material.

Acknowledgments

We thank A. Veillette for generously providing PEP antisera, A. MacDonald for supplying *S. mansoni* eggs, R. Guabiraba for histological assessment, and R. Salmond, S. Caserta, and J. Borger for helpful comments on the manuscript.

Funding: This project was supported by funding from the Arthritis Research UK Project grant #16409 (to L.M. and R.Z.), Arthritis Research UK Project grant #19652 (to AC, LS and RZ), the Wellcome Trust Project grant #086054 (to R.B., A.C., and R.Z.), the Wellcome Trust Investigator Award #096669 (to R.Z.) and the Swedish Medical Council K2010-80P-21592-01-4 (to L.S.). This work was also supported by a Strategic award from the Wellcome Trust for the Centre for Immunity, Infection and Evolution (Grant reference 095831).

References

1. Rhee I, Veillette A. Protein tyrosine phosphatases in lymphocyte activation and autoimmunity. Nat Immunol. 2012; 13:439–447. [PubMed: 22513334]
2. Cloutier JF, Veillette A. Cooperative inhibition of T-cell antigen receptor signaling by a complex between a kinase and a phosphatase. The Journal of experimental medicine. 1999; 189:111–121. [PubMed: 9874568]
3. Wu J, Katrekar A, Honigberg LA, Smith AM, Conn MT, Tang J, Jeffery D, Mortara K, Sampang J, Williams SR, Buggy J, et al. Identification of substrates of human protein-tyrosine phosphatase PTPN22. J Biol Chem. 2006; 281:11002–11010. [PubMed: 16461343]
4. Bottini N, Vang T, Cucca F, Mustelin T. Role of PTPN22 in type 1 diabetes and other autoimmune diseases. Semin Immunol. 2006; 18:207–213. [PubMed: 16697661]
5. Begovich AB, Carlton VEH, Honigberg LA, Schrodi SJ, Chokkalingam AP, Alexander HC, Ardlie KG, Huang Q, Smith AM, Spoerke JM, Conn MT, et al. A missense single-nucleotide

Europe PMC Funders Author Manuscripts

polymorphism in a gene encoding a protein tyrosine phosphatase (PTPN22) is associated with rheumatoid arthritis. Am J Hum Genet. 2004; 75:330–337. [PubMed: 15208781]

6. Bottini N, Musumeci L, Alonso A, Rahmouni S, Nika K, Rostamkhani M, MacMurray J, Meloni GF, Lucarelli P, Pellecchia M, Eisenbarth GS, et al. A functional variant of lymphoid tyrosine phosphatase is associated with type I diabetes. Nature genetics. 2004; 36:337–338. [PubMed: 15004560]
7. Zhang J, Zahir N, Jiang Q, Miliotis H, Heyraud S, Meng X, Dong B, Xie G, Qiu F, Hao Z, McCulloch CA, et al. The autoimmune disease-associated PTPN22 variant promotes calpain-mediated Lyp/Pep degradation associated with lymphocyte and dendritic cell hyperresponsiveness. Nature genetics. 2011; 43:902–907. [PubMed: 21841778]
8. Zikherman J, Hermiston M, Steiner D, Hasegawa K, Chan A, Weiss A. PTPN22 Deficiency Cooperates with the CD45 E613R Allele to Break Tolerance on a Non-Autoimmune Background. The Journal of Immunology. 2009; 182:4093–4106. [PubMed: 19299707]
9. Fiorillo E, Orrú V, Stanford SM, Liu Y, Salek M, Rapini N, Schenone AD, Saccucci P, Delogu LG, Angelini F, Manca Bitti ML, et al. Autoimmune-associated PTPN22 R620W variation reduces phosphorylation of lymphoid phosphatase on an inhibitory tyrosine residue. J Biol Chem. 2010; 285:26506–26518. [PubMed: 20538612]
10. Rieck M, Arechiga A, Onengut-Gumuscu S, Greenbaum C, Concannon P, Buckner JH. Genetic variation in PTPN22 corresponds to altered function of T and B lymphocytes. J Immunol. 2007; 179:4704–4710. [PubMed: 17878369]
11. Vang T, Congia M, Macis MD, Musumeci L, Orru V, Zavattari P, Nika K, Tautz L, Tasken K, Cucca F, Mustelin T, et al. Autoimmune-associated lymphoid tyrosine phosphatase is a gain-of-function variant. Nature genetics. 2005; 37:1317–1319. [PubMed: 16273109]
12. Negro R, Gobessi S, Longo PG, He Y, Zhang ZY, Laurenti L, Efremov DG. Overexpression of the autoimmunity-associated phosphatase PTPN22 promotes survival of antigen-stimulated chronic lymphocytic leukemia cells by selectively activating the AKT pathway. Blood. 2012; 119:6278–6287. [PubMed: 22569400]
13. Menard L, Saadoun D, Isnardi I, Ng YS, Meyers G, Massad C, Price C, Abraham C, Motaghedi R, Buckner JH, Gregersen PK, et al. The PTPN22 allele encoding an R620W variant interferes with the removal of developing autoreactive B cells in humans. The Journal of clinical investigation. 2011; 121:3635–3644. [PubMed: 21804190]
14. Hasegawa K, Martin F, Huang G, Tumas D, Diehl L, Chan AC. PEST domain-enriched tyrosine phosphatase (PEP) regulation of effector/memory T cells. Science. 2004; 303:685–689. [PubMed: 14752163]
15. Au-Yeung BB, Levin SE, Zhang C, Hsu L-Y, Cheng DA, Killeen N, Shokat KM, Weiss A. A genetically selective inhibitor demonstrates a function for the kinase Zap70 in regulatory T cells independent of its catalytic activity. Nature immunology. 2010; 11:1085–1092. [PubMed: 21037577]
16. Surh CD, Sprent J. Homeostasis of naive and memory T cells. Immunity. 2008; 29:848–862. [PubMed: 19100699]
17. Malissen B, Aguado E, Malissen M. Role of the LAT adaptor in T-cell development and Th2 differentiation. Advances in immunology. 2005; 87:1–25. [PubMed: 16102570]
18. Ranger AM, Oukka M, Rengarajan J, Glimcher LH. Inhibitory function of two NFAT family members in lymphoid homeostasis and Th2 development. Immunity. 1998; 9:627–635. [PubMed: 9846484]
19. Wing K, Sakaguchi S. Regulatory T cells exert checks and balances on self tolerance and autoimmunity. Nature immunology. 2010; 11:7–13. [PubMed: 20016504]
20. Chen W, Jin W, Hardegen N, Lei KJ, Li L, Marinos N, McGrady G, Wahl SM. Conversion of peripheral CD4+CD25- naive T cells to CD4+CD25+ regulatory T cells by TGF-beta induction of transcription factor Foxp3. The Journal of experimental medicine. 2003; 198:1875–1886. [PubMed: 14676299]
21. Zheng Y, Josefowicz S, Chaudhry A, Peng XP, Forbush K, Rudensky AY. Role of conserved non-coding DNA elements in the Foxp3 gene in regulatory T-cell fate. Nature. 2010; 463:808–812. [PubMed: 20072126]

Europe PMC Funders Author Manuscripts

22. Marson A, Kretschmer K, Frampton GM, Jacobsen ES, Polansky JK, MacIsaac KD, Levine SS, Fraenkel E, von Boehmer H, Young RA. Foxp3 occupancy and regulation of key target genes during T-cell stimulation. Nature. 2007; 445:931–935. [PubMed: 17237765]
23. Barrett JC, Hansoul S, Nicolae DL, Cho JH, Duerr RH, Rioux JD, Brant SR, Silverberg MS, Taylor KD, Barmada MM, Bitton A, et al. Genome-wide association defines more than 30 distinct susceptibility loci for Crohn's disease. Nat Genet. 2008; 40:955–962. [PubMed: 18587394]
24. Franke A, McGovern DP, Barrett JC, Wang K, Radford-Smith GL, Ahmad T, Lees CW, Balschun T, Lee J, Roberts R, Anderson CA, et al. Genome-wide meta-analysis increases to 71 the number of confirmed Crohn's disease susceptibility loci. Nat Genet. 2010; 42:1118–1125. [PubMed: 21102463]
25. Hue S, Ahern P, Buonocore S, Kullberg MC, Cua DJ, McKenzie BS, Powrie F, Maloy KJ. Interleukin-23 drives innate and T cell-mediated intestinal inflammation. The Journal of experimental medicine. 2006; 203:2473–2483. [PubMed: 17030949]
26. Shevach EM. Mechanisms of foxp3+ T regulatory cell-mediated suppression. Immunity. 2009; 30:636–645. [PubMed: 19464986]
27. Fisson S, Darrasse-Jeze G, Litvinova E, Septier F, Klatzmann D, Liblau R, Salomon BL. Continuous activation of autoreactive CD4+ CD25+ regulatory T cells in the steady state. The Journal of experimental medicine. 2003; 198:737–746. [PubMed: 12939344]
28. Lehmann J, Huehn J, de la Rosa M, Maszyna F, Kretschmer U, Krenn V, Brunner M, Scheffold A, Hamann A. Expression of the integrin alpha Ebeta 7 identifies unique subsets of CD25+ as well as CD25- regulatory T cells. Proc Natl Acad Sci U S A. 2002; 99:13031–13036. [PubMed: 12242333]
29. Fontenot JD, Rasmussen JP, Gavin MA, Rudensky AY. A function for interleukin 2 in Foxp3-expressing regulatory T cells. Nature immunology. 2005; 6:1142–1151. [PubMed: 16227984]
30. Rubtsov YP, Rasmussen JP, Chi EY, Fontenot J, Castelli L, Ye X, Treuting P, Siewe L, Roers A, Henderson WR Jr, Muller W, et al. Regulatory T cell-derived interleukin-10 limits inflammation at environmental interfaces. Immunity. 2008; 28:546–558. [PubMed: 18387831]
31. Gavin MA, Clarke SR, Negrou E, Gallegos A, Rudensky A. Homeostasis and anergy of CD4(+)CD25(+) suppressor T cells in vivo. Nature immunology. 2002; 3:33–41. [PubMed: 11740498]
32. Hickman SP, Yang J, Thomas RM, Wells AD, Turka LA. Defective activation of protein kinase C and Ras-ERK pathways limits IL-2 production and proliferation by CD4+CD25+ regulatory T cells. J Immunol. 2006; 177:2186–2194. [PubMed: 16887978]
33. Marski M, Kandula S, Turner JR, Abraham C. CD18 is required for optimal development and function of CD4+CD25+ T regulatory cells. J Immunol. 2005; 175:7889–7897. [PubMed: 16339524]
34. Wohler J, Bullard D, Schoeb T, Barnum S. LFA-1 is critical for regulatory T cell homeostasis and function. Mol Immunol. 2009; 46:2424–2428. [PubMed: 19428111]
35. Yu X, Chen M, Zhang S, Yu ZH, Sun JP, Wang L, Liu S, Imasaki T, Takagi Y, Zhang ZY. Substrate specificity of lymphoid-specific tyrosine phosphatase (Lyp) and identification of Src kinase-associated protein of 55 kDa homolog (SKAP-HOM) as a Lyp substrate. The Journal of biological chemistry. 2011; 286:30526–30534. [PubMed: 21719704]
36. Maine CJ, Hamilton-Williams EE, Cheung J, Stanford SM, Bottini N, Wicker LS, Sherman LA. PTPN22 Alters the Development of Regulatory T Cells in the Thymus. Journal of immunology. 2012; 188:5267–5275.
37. Grinberg-Bleyer Y, Saadoun D, Baeyens A, Billiard F, Goldstein JD, Gregoire S, Martin GH, Elhage R, Derian N, Carpentier W, Marodon G, et al. Pathogenic T cells have a paradoxical protective effect in murine autoimmune diabetes by boosting Tregs. The Journal of clinical investigation. 2010; 120:4558–4568. [PubMed: 21099113]
38. McNeill L, Salmond RJ, Cooper JC, Carret CK, Cassady-Cain RL, Roche-Molina M, Tandon P, Holmes N, Alexander DR. The differential regulation of Lck kinase phosphorylation sites by CD45 is critical for T cell receptor signaling responses. Immunity. 2007; 27:425–437. [PubMed: 17719247]

39. Arimura Y, Vang T, Tautz L, Williams S, Mustelin T. TCR-induced downregulation of protein tyrosine phosphatase PEST augments secondary T cell responses. Mol Immunol. 2008; 45:3074–3084. [PubMed: 18457880]

40. Stefanova I, Hemmer B, Vergelli M, Martin R, Biddison WE, Germain RN. TCR ligand discrimination is enforced by competing ERK positive and SHP-1 negative feedback pathways. Nature immunology. 2003; 4:248–254. [PubMed: 12577055]

41. Davidson D, Shi X, Zhong M-C, Rhee I, Veillette A. The Phosphatase PTP-PEST Promotes Secondary T Cell Responses by Dephosphorylating the Protein Tyrosine Kinase Pyk2. Immunity. 2010; 33:167–180. [PubMed: 20727793]

Europe PMC Funders Author Manuscripts

Europe PMC Funders Author Manuscripts

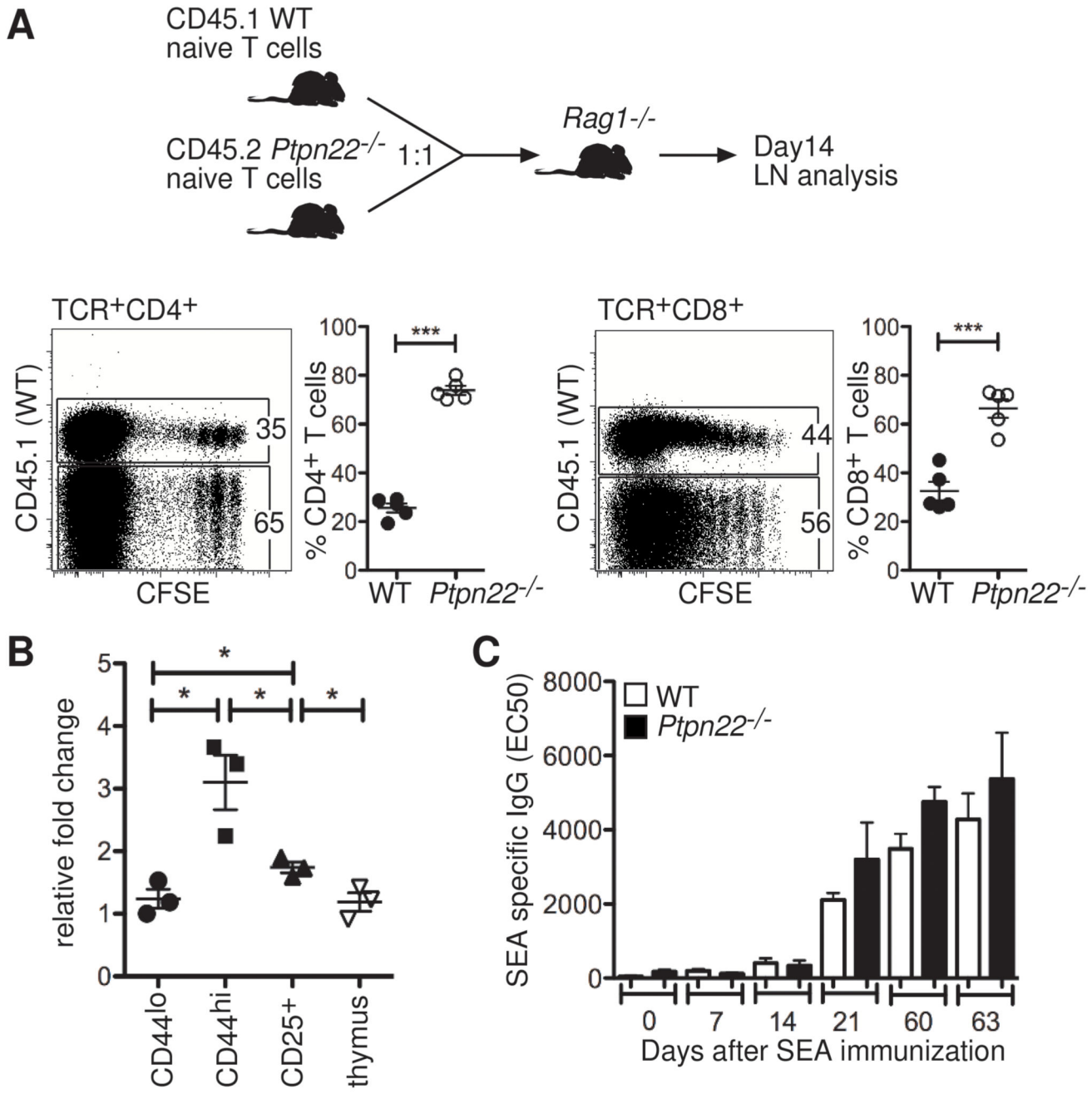

Fig. 1. *Ptpn22*$^{-/-}$ T cells show greater expansion in numbers than do WT cells in vivo, but they do not have increased T_H2 helper activity.

(**A**) Naïve T cells purified from WT (CD45.1$^+$) and *Ptpn22*$^{-/-}$ (CD45.2$^+$) lymph nodes were labeled with CFSE and injected i.v. into *Rag1*$^{-/-}$ recipient mice (n = 5) at a 1:1 ratio (4 x 10^6 cells/mouse in total). The abundances of CD44 and CD25 on the surface of transferred T cells were comparable before injection, and the proportions of WT (CD45.1$^+$) and *Ptpn22*$^{-/-}$ (CD45.2$^+$) cells in the blood of recipients were monitored on day 1 (WT = 53 ± 8% and *Ptpn22*$^{-/-}$ = 43 ± 9%; values are means ± SD). After 14 days, the lymph nodes of recipient

Europe PMC Funders Author Manuscripts
Europe PMC Funders Author Manuscripts

Europe PMC Funders Author Manuscripts

Europe PMC Funders Author Manuscripts

mice were analyzed by flow cytometry for the proportions of $CD45.1^+$ and $CD45.2^+$ T cells. Representative dot plots and ratios of WT ($CD45.1^+$) to *Ptpn22*$^{-/-}$ ($CD45.1^-$) cells are shown. Each point represents an individual animal; data are means ± SEM. Results are representative of two individual experiments. (**B**) Amounts of *PTPN22* mRNA were assessed in $CD4^+$ T cells from lymph nodes of WT mice that were sorted to give $CD25^-CD44^{lo}$, $CD25^-CD44^{hi}$, and $CD25^+$ cells, as well as in total thymus cells. Values are expressed relative to the amounts of *Hprt* mRNA. Each point represents an individual animal (n = 3 mice). (**C**) Groups of WT and *Ptpn22*$^{-/-}$ mice (n = 5 mice of each genotype) were immunized with 2000 *S. mansoni* eggs on day 0, followed by a boost of 1000 eggs on day 49. Sera from tail bleeds were assessed for SEA-specific IgG at various time points by ELISA. Graph represents the mean EC50 values values ± SEM. $*P < 0.05$, $***P < 0.005$.

Europe PMC Funders Author Manuscripts

Europe PMC Funders Author Manuscripts

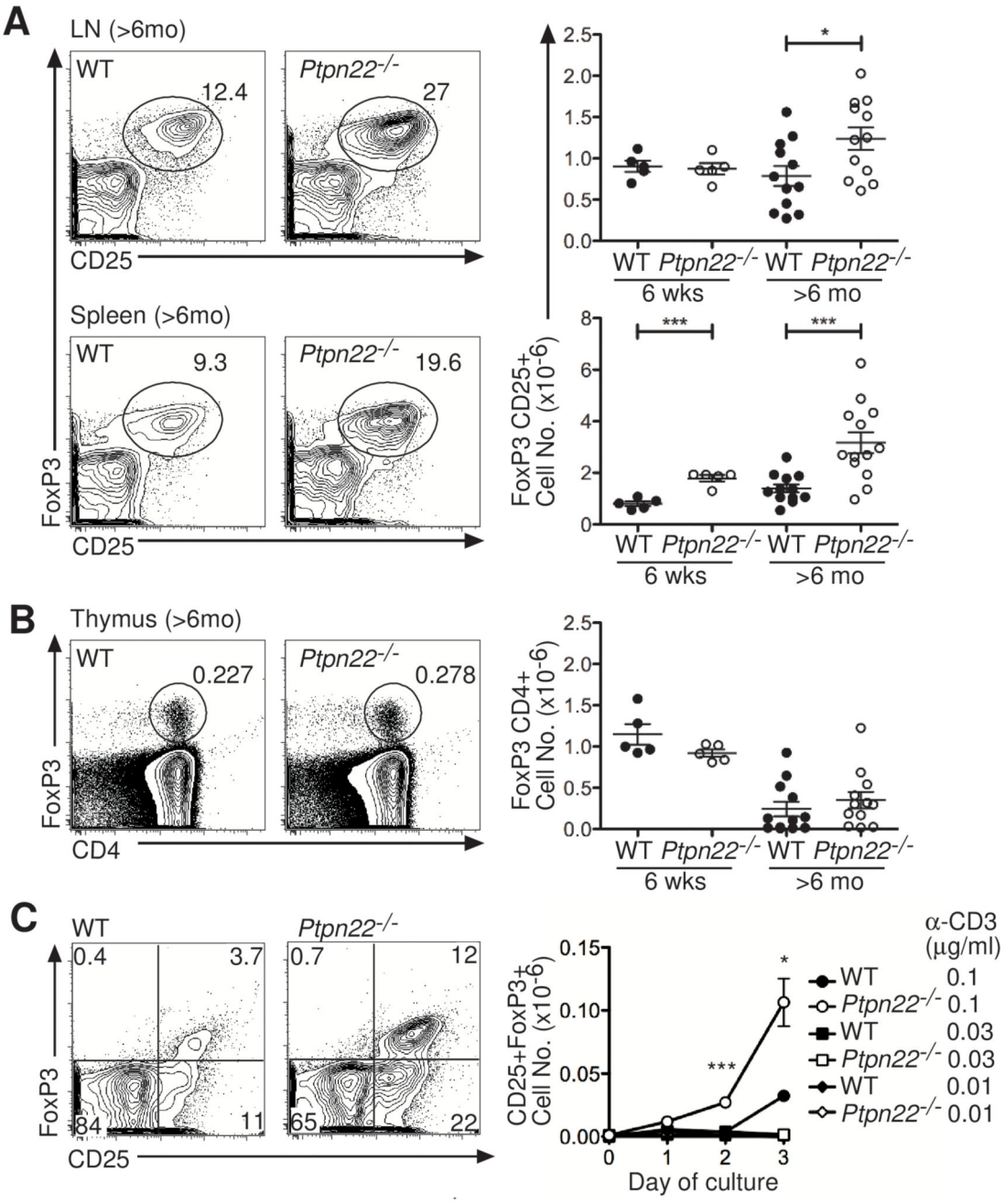

Fig. 2. *Ptpn22*$^{-/-}$ mice have increased proportions and numbers of Tregs.

(**A** and **B**) Flow cytometry was used to determine the proportions and total numbers of $CD4^+FoxP3^+CD25^+$ Tregs in (A) lymph nodes (LN) and spleens and (B) thymi of young (6 weeks) and old (>6 mo) WT and *Ptpn22*$^{-/-}$ mice. Representative dot plots show the percentages of Tregs in individual old mice. Graphs show lymph nodes and spleens from multiple mice, with points representing individual mice together with the mean ± SEM. (**C**) FoxP3 abundance was analyzed daily by flow cytometry after stimulation of naïve $CD4^+CD25^-$ T cells in vitro with a range of concentrations of anti-CD3 (0.01, 0.3 and 0.1

μg/ml) antibody together with anti-CD28 (0.2 μg/ml), IL-2 (20 ng/ml), and TGF-β (0.4 ng/ml). Representative plots illustrate the proportions of $FoxP3^+CD25^+$ cells after culture with anti-CD3 antibody (0.1 μg/ml) for 3 days. Graph shows the mean ± SEM of the absolute numbers of $FoxP3^+CD25^+$ cells from triplicate wells of 3 pooled mice, and is representative of 3 experiments. The fold-increase in the mean fluorescence intensity (MFI) of FoxP3 in *Ptpn22*$^{-/-}$ iTregs compared to that of WT iTregs after 3 days in culture with anti-CD3 antibody (0.1 μg/ml) was 1.2, 1.3, and 1.5 in 3 experiments. *$P < 0.05$, ***$P < 0.0005$.

Europe PMC Funders Author Manuscripts

Europe PMC Funders Author Manuscripts

Europe PMC Funders Author Manuscripts

Europe PMC Funders Author Manuscripts

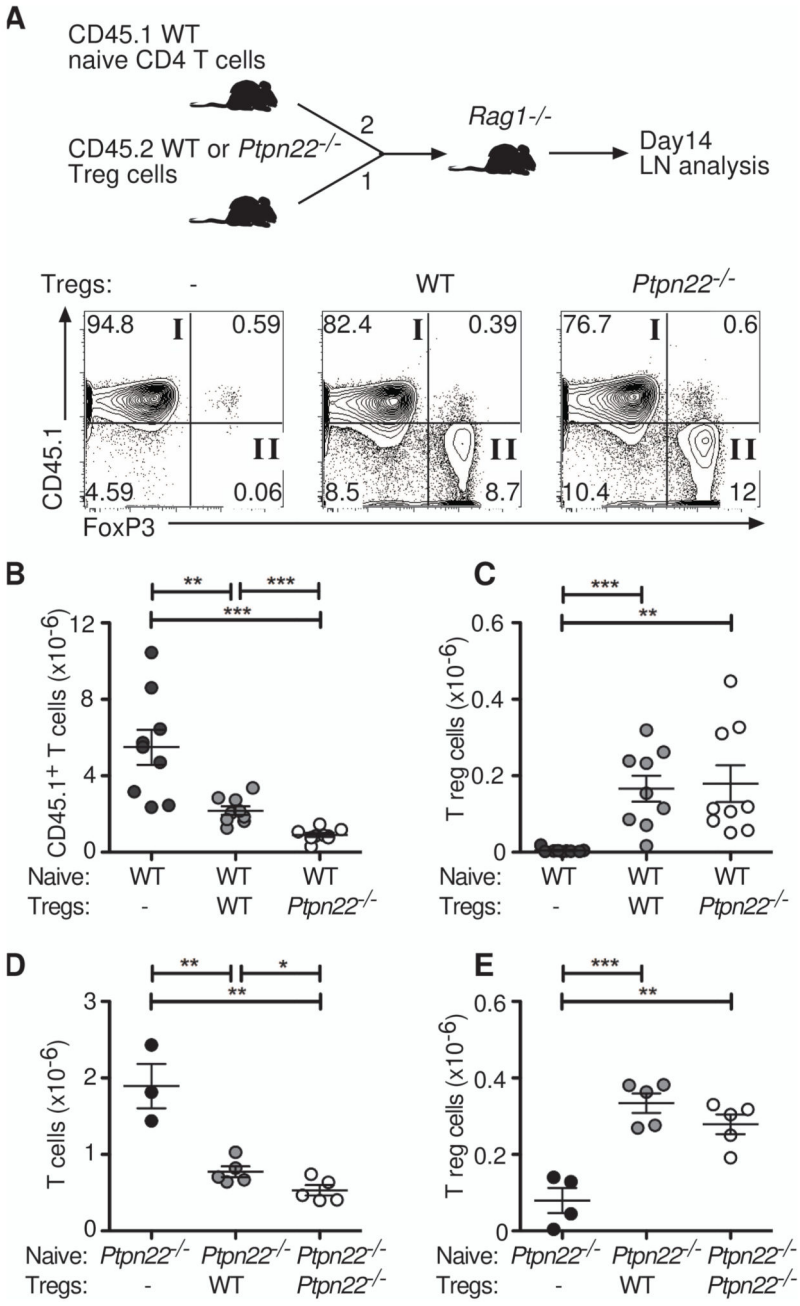

Fig. 3. *Ptpn22*$^{-/-}$ Tregs are more suppressive than WT Tregs in vivo.

(**A** to **C**) WT naïve CD45.1^{+}CD4^{+}CD25^{-}CD44^{lo} cells (4 x 10^{5}) were injected alone or together with WT or *Ptpn22*$^{-/-}$ CD45.2^{+}CD4^{+}CD25^{+} Tregs (2 x 10^{5}) i.v. into *Rag1*$^{-/-}$ recipients in a 2:1 ratio as indicated (n = 9 mice per group). After 14 days, lymph nodes were assessed by flow cytometry for their proportions of CD45.1^{+}FoxP3^{-} cells (quadrant I) and CD45.1^{-}FoxP3^{+} Tregs (quadrant II). Representative plots are shown from each group. Absolute numbers of (B) CD45.1^{+}FoxP3^{-} cells and (C) CD45.1^{-}FoxP3^{+} Treg are shown. Each symbol represents an individual mouse. Bars represent SEM. Data are representative of

3 individual experiments. (**D** and **E**) *Ptpn22*$^{-/-}$ naïve CD4^{+}CD25^{-}CD44^{lo} cells (1 x 10^{5}) were injected alone or together with WT or *Ptpn22*$^{-/-}$ thymic CD4^{+}CD25^{+} Tregs (0.25 x 10^{5}) i.v. into *Rag1*$^{-/-}$ recipients in a 4:1 ratio (n = 3-5 mice per group). After 19 days, lymph nodes were assessed for the numbers of (D) FoxP3^{-} cells and (E) FoxP3^{+} Tregs. Each symbol represents an individual mouse. Bars represent SEM. Data are representative of 2 individual experiments. $^{**}P < 0.005$, $^{***}P < 0.0005$.

Europe PMC Funders Author Manuscripts

Europe PMC Funders Author Manuscripts

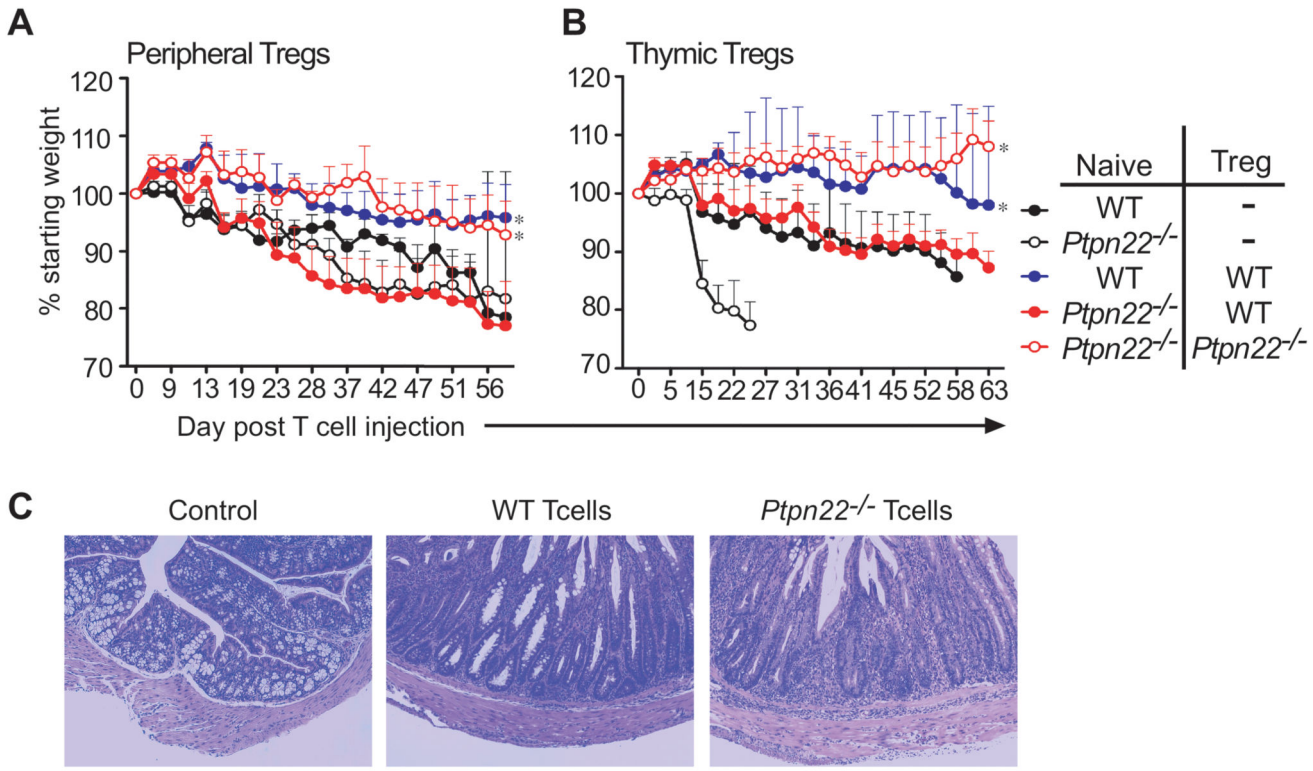

Fig. 4. Colitis induced by pathogenic *Ptpn22*$^{-/-}$ effector T cells can be controlled by *Ptpn22*$^{-/-}$, but not WT, Tregs.

(**A** and **B**) Groups of *Rag1*$^{-/-}$ recipients (n = 4 or 5 mice) were injected i.v. with either WT or *Ptpn22*$^{-/-}$ naïve CD4^{+}CD25^{-}CDRB^{hi} cells (4 x 10^{5}) alone or together with WT or *Ptpn22*$^{-/-}$ CD4^{+}CD25^{+} Tregs (5 x 10^{4}) obtained from (A) peripheral lymph nodes or (B) thymus in a ratio of 8:1. Mice were assessed for weight loss for up to 70 days after injection, and percentage weight loss is shown. Survival of protected WT/WT and *Ptpn22*$^{-/-}$/*Ptpn22*$^{-/-}$ groups was significantly different from that of all other groups; *$P < 0.05$. (**C**) To confirm that similar pathology was induced by WT and *Ptpn22*$^{-/-}$ colitic T cells, lower intestine sections taken from experimental mice underwent histological analysis. Microphotographs of sections of lower intestine from a representative control C57/BL6 (no injected cells) mouse, a *Rag1*$^{-/-}$ recipient injected with WT CD4^{+}CD25^{-}CDRB^{hi} T cells, and a *Rag1*$^{-/-}$ recipient injected with *Ptpn22*$^{-/-}$ CD4^{+}CD25^{-}CDRB^{hi} T cells are shown.

Europe PMC Funders Author Manuscripts
Europe PMC Funders Author Manuscripts

Europe PMC Funders Author Manuscripts

Europe PMC Funders Author Manuscripts

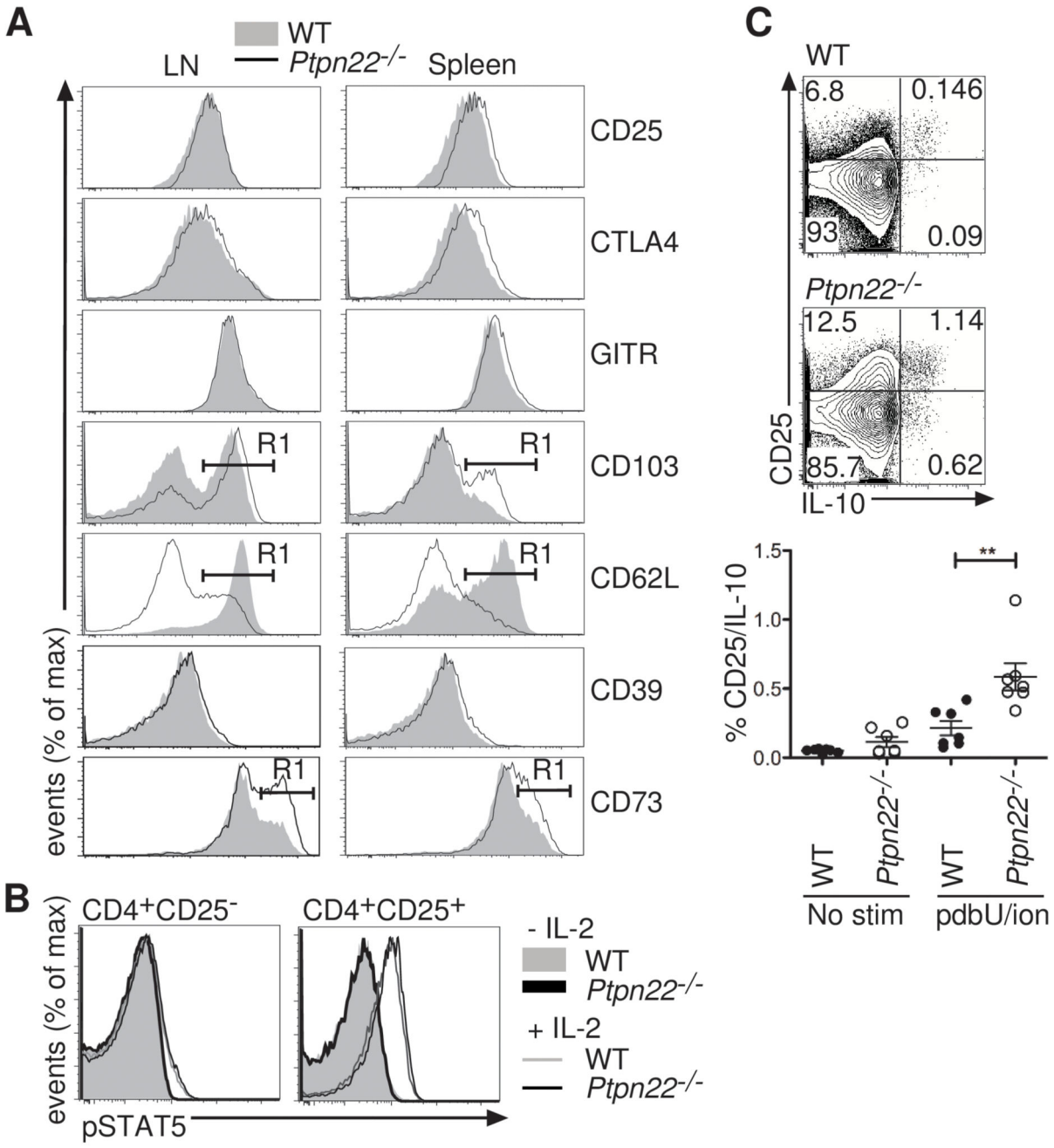

Fig. 5. *Ptpn22*$^{-/-}$ Tregs have an activated phenotype.

(**A**) CD4^{+}FoxP3^{+}CD25^{+} cells from lymph nodes and spleen were stained with antibodies to detect surface CD25, CD103, CD62L, CD39, and CD73 as well as intracellular GITR and CTLA-4 by flow cytometry. The %±SD of lymph node and splenic Tregs positive for the markers CD103, CD62L and CD73 as indicated by gate R1 (shown on histogram) is given in Table S1. Representative histograms of 5 mice from each group are shown. (**B**) The abundance of pSTAT5 was assessed in WT and *Ptpn22*$^{-/-}$ Tregs after stimulation with IL-2. WT CD4^{+}CD45.1^{+} cells were mixed in a 1:1 ratio with CD4^{+}CD45.2^{+} *Ptpn22*$^{-/-}$ cells, and

were stimulated with IL-2 (1 ng/ml) for 15 min before being fixed and stained for CD45.1, CD45.2, CD4, CD25, and pSTAT5. Representative histograms show the abundance of pSTAT5 in WT and *Ptpn22*$^{-/-}$ CD25^{-} and CD25^{+} cells with (open histogram) and without (filled histogram) IL-2. Data are representative of 2 experiments. (**C**) IL-10 production from CD4+CD25+ WT and *Ptpn22*$^{-/-}$ Tregs was measured after incubation of lymph node cells without (no stim) or with PDBU and ionomycin for 4 hours. Representative plots of stimulated cells are shown, and the graph represents the percentages of IL-10^{+}CD25^{+} cells from individual animals (n = 7 mice, $^{**}P < 0.005$).

Europe PMC Funders Author Manuscripts

Europe PMC Funders Author Manuscripts

Europe PMC Funders Author Manuscripts

Europe PMC Funders Author Manuscripts

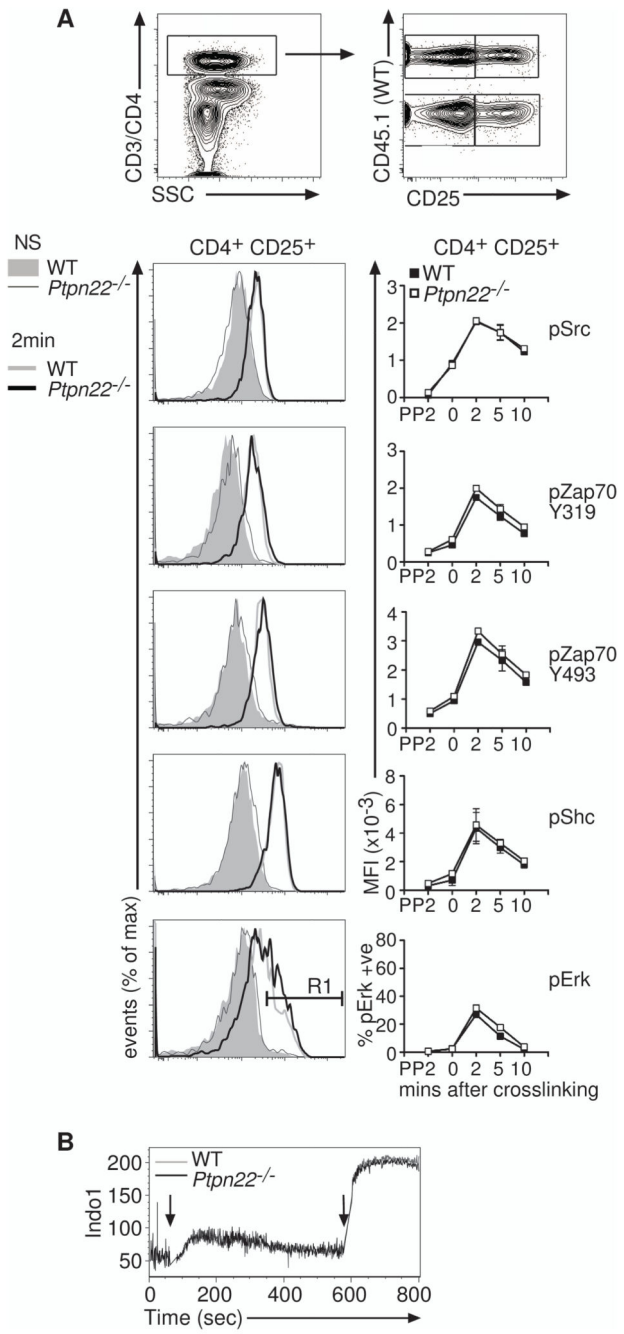

Fig. 6. *Ptpn22*$^{-/-}$ Tregs show no enhancement of signaling after TCR stimulation.

(**A**) WT CD45.1^{+} lymph node cells were mixed 1:1 with CD45.2^{+} *Ptpn22*$^{-/-}$ lymph node cells and stimulated with biotinylated anti-CD3 and anti-CD4 antibodies, which were crosslinked with streptavidin-PerCP. Cells were fixed, permeabilized, and stained with anti-CD25, anti-CD45.1, anti-CD45.2, and phospho-specific antibodies, as indicated. Example dot plots indicating the gating strategy and representative histograms show the data 2 mins after cross-linking. Data are representative of 3 individual experiments. (**B**) Ca^{2+} flux in WT and *Ptpn22*$^{-/-}$ CD4+CD25+ Tregs after cross-linking of CD3 and CD4 was measured by

flow cytometry. INDO-1–loaded WT ($CD45.1^+$) and *Ptpn22*$^{-/-}$ ($CD45.2^+$) cells were mixed 1:1 and labeled with biotinylated anti-CD3 and anti-CD4 antibodies, which were crosslinked by the addition of streptavidin (first arrow). After 10 mins, ionomycin was added to the tubes to elicit maximum Ca^{2+} flux. Representative traces for Ca^{2+} flux are shown from one of two replicate experiments.

Europe PMC Funders Author Manuscripts

Europe PMC Funders Author Manuscripts

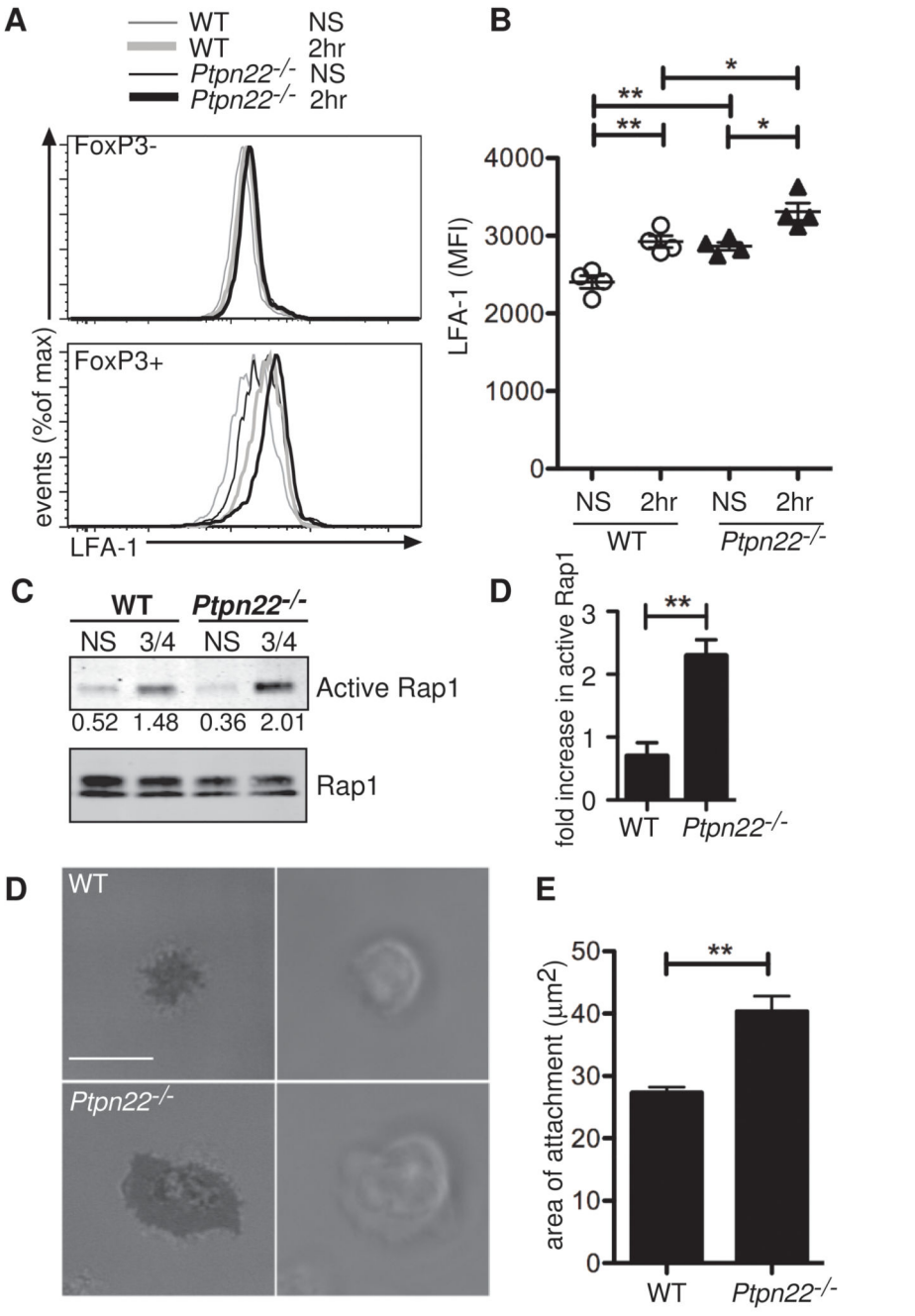

Fig. 7. *Ptpn22*$^{-/-}$ Tregs have increased amounts of LFA1 and make larger areas of contact with surface bound ICAM1 than do WT Tregs.

(**A** and **B**) WT and *Ptpn22*$^{-/-}$ CD4^{+} cells were stained with biotinylated anti-CD3 and anti-CD4 antibodies, which were then cross-linked with streptavidin for 2 hours at 37°C, and then cells were assessed by flow cytometry for LFA1 abundance. Tregs were identified by detection of FoxP3 after staining for LFA1. (A) Representative histograms show LFA1 abundance before and after cross-linking of CD3 and CD4 in both FoxP3^{-} and FoxP3^{+} T cells. (B) MFIs of LFA1 in FoxP3^{+} cells are represented graphically with each point representing an individual animal (n = 4 mice). (**C**) In vitro–derived WT and *Ptpn22*$^{-/-}$ CD4^{+}

Europe PMC Funders Author Manuscripts
Europe PMC Funders Author Manuscripts

effector T cells were incubated with biotinylated anti-CD3 and anti-CD4 antibodies, which were cross-linked with avidin for 5 min at 37°C, and then cells were assessed for active Rap1 by immunoprecipitation. Normalized band intensities are indicated. Data are representative of 3 independent experiments. (**D**) Quantification of data shown in (C). $^{**}P < 0.005$. (**E**) $CD4^+CD25^+$ cells were sorted from the lymph nodes of WT and *Ptpn22*$^{-/-}$ mice and were allowed to adhere to ICAM1-coated slides before being visualized by IRM. (Scale bar: 10 μm). (**F**) Quantification of the area of contact made by the Tregs is shown. Bars represent SEM. Data are representative of 3 individual animals of each genotype and two separate experiments.

Europe PMC Funders Author Manuscripts

Europe PMC Funders Author Manuscripts